MR Imaging Radiomics Signatures for Predicting the Risk of Breast Cancer Recurrence as Given by Research Versions of MammaPrint, Oncotype DX, and PAM50 Gene Assays[1]

Hui Li, PhD
Yitan Zhu, PhD
Elizabeth S. Burnside, MD, MPH, MS
Karen Drukker, PhD, MBA
Katherine A. Hoadley, PhD
Cheng Fan, MS
Suzanne D. Conzen, MD
Gary J. Whitman, MD
Elizabeth J. Sutton, MD
Jose M. Net, MD
Marie Ganott, MD
Erich Huang, PhD
Elizabeth A. Morris, MD
Charles M. Perou, PhD
Yuan Ji, PhD
Maryellen L. Giger, PhD

© RSNA, 2016

Purpose: To investigate relationships between computer-extracted breast magnetic resonance (MR) imaging phenotypes with multigene assays of MammaPrint, Oncotype DX, and PAM50 to assess the role of radiomics in evaluating the risk of breast cancer recurrence.

Materials and Methods: Analysis was conducted on an institutional review board–approved retrospective data set of 84 deidentified, multi-institutional breast MR examinations from the National Cancer Institute Cancer Imaging Archive, along with clinical, histopathologic, and genomic data from The Cancer Genome Atlas. The data set of biopsy-proven invasive breast cancers included 74 (88%) ductal, eight (10%) lobular, and two (2%) mixed cancers. Of these, 73 (87%) were estrogen receptor positive, 67 (80%) were progesterone receptor positive, and 19 (23%) were human epidermal growth factor receptor 2 positive. For each case, computerized radiomics of the MR images yielded computer-extracted tumor phenotypes of size, shape, margin morphology, enhancement texture, and kinetic assessment. Regression and receiver operating characteristic analysis were conducted to assess the predictive ability of the MR radiomics features relative to the multigene assay classifications.

Results: Multiple linear regression analyses demonstrated significant associations (R^2 = 0.25–0.32, r = 0.5–0.56, P < .0001) between radiomics signatures and multigene assay recurrence scores. Important radiomics features included tumor size and enhancement texture, which indicated tumor heterogeneity. Use of radiomics in the task of distinguishing between good and poor prognosis yielded area under the receiver operating characteristic curve values of 0.88 (standard error, 0.05), 0.76 (standard error, 0.06), 0.68 (standard error, 0.08), and 0.55 (standard error, 0.09) for MammaPrint, Oncotype DX, PAM50 risk of relapse based on subtype, and PAM50 risk of relapse based on subtype and proliferation, respectively, with all but the latter showing statistical difference from chance.

Conclusion: Quantitative breast MR imaging radiomics shows promise for image-based phenotyping in assessing the risk of breast cancer recurrence.

© RSNA, 2016

Online supplemental material is available for this article.

Advances in gene expression profiling by using microarray-based technologies have allowed investigators to study the complexity of breast tumors (1–9). Various investigators have used and developed methods for gene expression analyses (1,2) to relate breast cancer expression profiles to prognosis and risk of recurrence. These include the 70-gene MammaPrint microarray assay (Agendia, Amsterdam, the Netherlands) (3,4), the 21-gene Oncotype DX assay (Genomic Health, Redwood City, Calif) (5–7) for predicting breast cancer recurrence, and the 50-gene PAM50 assay (Prosigna; Nanostring Technologies, Seattle, Wash) (8,9) for identifying clinically relevant molecular subtypes of breast cancer. Outputs from such multiple-gene assays are expected to be useful in the management of breast cancer by predicting prognosis and/or effectiveness of treatment.

Methods for computer-aided diagnosis and quantitative characterization—that is, image-based tumor phenotyping—of cancers on breast images (obtained with mammography, ultrasonography, and magnetic resonance [MR] imaging) have been in development for decades (10–12) and have recently received a renewed interest with the expansion beyond detection and diagnosis. Image-based tumor phenotypes by using computer vision techniques are being evaluated in terms of their relationship to breast cancer invasiveness, stage, lymph node involvement, molecular subtypes (11–18), and genomics (19–23).

Researchers involved with The Cancer Genome Atlas (TCGA) have demonstrated the role of gene expression profiles in characterizing TCGA breast cancer (24). In addition, the National Cancer Institute started collecting the corresponding MR imaging data for some TCGA tumors and having the data stored within The Cancer Imaging Archive (TCIA) (25). The purpose of our study was to investigate the relationships between breast MR computer-extracted image phenotypes (CEIPs) with gene expression assays of MammaPrint, Oncotype DX, and PAM50 to assess the potential role of MR imaging radiomics in evaluating the risk of breast cancer recurrence.

Materials and Methods

Study Population and MR Images

Patient data were obtained from the National Cancer Institute TCGA Breast Invasive Carcinoma and TCIA initiatives according to institutional review board–approved, Health Insurance Portability and Accountability Act–compliant protocols. Analyses were conducted on deidentified data only. Thus, patient selection basically included all cases available through the TCGA TCIA repository. Although this data set of MR images is not state of the art in terms current clinical protocols, it is unique in that by being part of the TCGA, assessment relative to gene assays and other genomic analyses is possible, which is not readily available in current clinical radiology departments.

At the time of our study, only 108 cases of the entire TCGA breast cancer data set had breast MR images, which had been collected and made available in the TCIA *(http://www.cancerimaging archive.net)* (25). However, to minimize variations in image quality across the multi-institutional cases, in our analysis, we included only breast MR imaging studies acquired with 1.5-T GE Medical

Advances in Knowledge

- Regression models of MR computer-extracted image phenotypes (CEIPs)—that is, breast MR imaging radiomics—are significantly associated with breast cancer risk of recurrence as predicted with research-based multigene assays, including MammaPrint, Oncotype DX, and PAM50 ($R^2 = 0.25$–0.32, $r = 0.50$–0.56, $P < .0001$); important CEIPs included tumor size, as well as enhancement texture patterns that potentially indicate tumor heterogeneity.

- Use of radiomics in the task of distinguishing between good and poor prognosis in terms of estimated risk of recurrence yielded area under the receiver operating characteristic curve values of 0.88 (standard error, 0.05), 0.76 (standard error, 0.06), 0.68 (standard error, 0.08), and 0.55 (standard error, 0.09) for MammaPrint, Oncotype DX, PAM50 risk of relapse based on subtype, and PAM50 risk of relapse based on subtype and proliferation, respectively.

Implications for Patient Care

- Quantitative breast MR imaging radiomics shows promise as a means for image-based tumor phenotyping in assessing the risk of breast cancer recurrence.

- Computerized MR imaging tumor phenotyping may yield quantitative predictive models of breast cancer for precision medicine and may potentially affect patient treatment strategy.

Table 1

Distribution of Cases in the Database: Tabulation of Receptor Status (ER, PR, and HER2), MammaPrint, Oncotype DX, and PAM50 Gene Assays of the Study Data Set

Gene Assay Test and Prognosis	Total (%)	ER Positive (%)	ER Negative (%)	PR Positive (%)	PR Negative (%)	HER2 Positive (%)	HER2 Negative (%)
All cases	…	87 (73/84)	13 (11/84)	80 (67/84)	20 (17/84)	23 (19/84)	77 (65/84)
MammaPrint							
Good prognosis	83 (70/84)	98 (69/70)	1 (1/70)	90 (63/70)	10 (7/70)	20 (14/70)	80 (56/70)
Bad prognosis	17 (14/84)	28 (4/14)	71 (10/14)	28 (4/14)	71 (10/14)	36 (5/14)	64 (9/14)
Oncotype DX							
Lowest tertile (lowest risk)	30 (25/84)	100 (25/25)	0 (0/25)	96 (24/25)	4 (1/25)	20 (5/25)	80 (20/25)
Middle tertile	38 (32/84)	100 (32/32)	0 (0/32)	97 (31/32)	3 (1/32)	9 (3/32)	91 (29/32)
Top tertile	32 (27/84)	59 (16/27)	41 (11/27)	44 (12/27)	56 (15/27)	41 (11/27)	59 (16/27)
PAM50 ROR-S							
Low recurrence risk	62 (52/84)	100 (52/52)	0 (0/52)	94 (49/52)	6 (3/52)	17 (9/52)	83 (43/52)
Medium recurrence risk	20 (17/84)	94 (16/17)	6 (1/17)	82 (14/17)	18 (3/17)	18 (3/17)	82 (14/17)
High recurrence risk	18 (15/84)	33 (5/15)	67 (10/15)	27 (4/15)	73 (11/15)	47 (7/15)	53 (8/15)
PAM50 ROR-P							
Low recurrence risk	40 (34/84)	100 (34/34)	0 (0/34)	97 (33/34)	3 (1/34)	24 (8/34)	76 (26/34)
Medium recurrence risk	44 (37/84)	89 (33/37)	11 (4/37)	81 (30/37)	19 (7/37)	16 (6/37)	84 (31/37)
High recurrence risk	15 (13/84)	46 (6/13)	54 (7/13)	31 (4/13)	69 (9/13)	38 (5/13)	62 (8/13)

Note.—Numbers in parentheses are the data used to calculate the percentages.

Systems imaging units (Milwaukee, Wis**)**. Our database excluded 14 studies performed by using Siemens imaging units (Malvern, Pa) and one study performed by using a 3-T GE Medical Systems imaging unit, thus resulting in a total of 93 cases. We then excluded cases that had missing images for the dynamic sequence (one patient) or that, at the time, did not have gene expression analysis findings available (eight patients). After adhering to these criteria, the study data set of 84 patients with invasive breast cancer was finalized, with MR imaging examinations conducted at four institutions: Memorial Sloan-Kettering Cancer Center, Mayo Clinic, University of Pittsburg Medical Center, and Roswell Park Cancer Institute. The number of cases contributed by each institution, respectively, were nine (date range, 1999–2002), five (date range, 1999–2003), 46 (date range, 1999–2004), and 24 (date range, 1999–2002). The cancers included 74 ductal (88%), eight lobular (10%), and two mixed (2%) cancers. Of these, 73 (87%) were estrogen receptor (ER) positive, 67 (80%) were progesterone receptor (PR) positive, and 19 (23%) were human epidermal growth factor receptor 2 (HER2) positive. This set of images can

be downloaded and cited in future works by using *http://dx.doi.org/10.7937/K9/ TCIA.2014.8SIPIY6G*. The mean age ± standard deviation of the 84 patients was 53.6 years ± 11.6, and the range was 29–82 years.

For each examination, T1-weighted dynamic contrast material–enhanced MR images were analyzed for this study, including one unenhanced and three to five contrast-enhanced images obtained by using a T1-weighted three-dimensional spoiled gradient-echo sequence with a gadolinium-based contrast agent (Omniscan; Nycomed-Amersham, Princeton, NJ). In-plane resolution ranged from 0.53 to 0.86 mm, spacing between sections ranged from 2 to 3 mm, flip angle was 10°, acquisition matrix was 256 × 192, and temporal resolution was approximately 110 seconds.

Images from each breast MR examination were reviewed, and the lesion was located independently by three of 11 breast radiologists who were members of the TCGA Breast Phenotype Research Group by using ClearCanvas software (ClearCanvas, Toronto, Ontario, Canada) (26). The breast imaging experience of the 11 radiologists ranged from 4 to 29 years (E.S.B., 14 years; G.J.W., 25

years; E.J.S., 4 years; J.M.N., 5 years; M.G., 29 years; and E.A.M., 25 years; the other five radiologists were nonauthors). The tumor location was determined by means of consensus by using the radiologist reviewer information. This location of the primary tumor in each MR examination was made available in the subsequent computerized quantitative image analysis.

Recurrence Scores Obtained with Multigene Assays

The genomic-based scores for the multigene assays that served as the reference standards were determined at the University of North Carolina, which yielded "research-based" MammaPrint, Oncotype DX, and PAM50 assays (Table 1). It is important to note that for these TCGA samples, the clinical assay results were not available—that is, only the "research-based" assay outputs were available. Each statistical model as described in the original gene assay articles (3–9) was applied to the messenger RNA sequencing data to obtain research-based bioinformatics estimates of the risk of recurrence scores. The assays were run on a set of 1030 tumors and 110 adjacent

normal samples, and the results were extracted for the 84 samples used. The relationships between the different gene assays—that is, the correlations between the continuous output values from the different "research-based" gene assays (the "reference standards" in this study)—showed relatively high Spearman correlations (approximately 0.81–0.87). However, the categorization of these values into low-, medium-, or high-risk groups yielded conflicting outputs from one of the three multigene tests (ie, Oncotype DX), most likely due to the application of the published assay thresholds based on quantitative real-time polymerase chain reaction on the messenger RNA sequencing expression data. Therefore, for this single assay, we simply put the patients into rank expression order and created tertiles, and we used these as the low-, intermediate-, and high-risk categories. When done this way, the results of the research-based Oncotype DX assay were in much greater agreement with those of the other two, as has been shown previously (27).

Cancer subtypes were determined by using the PAM50 classifier (8). The training set used in the reference PAM50 algorithm had been composed of 50% ER-positive samples. In the TCGA data set, however, there were approximately 80% ER-positive samples. To normalize the TCGA data similarly to the PAM50 training set, TCGA messenger RNA sequencing data were subsampled for a group of cases that were 50% ER positive (freeze date, September 7, 2012; including 157 ER-positive and 157 randomly selected ER-positive cases). The median gene expression value for the subset was determined and applied to the full TCGA data set prior to running the PAM50 algorithm (8). There were 55 luminal A cancers, 10 luminal B cancers, five HER2-enriched cancers, 10 basal-like cancers, and four normal-like cancers in this study. Both risk of relapse based on subtype (ROR-S) and risk of relapse based on subtype and proliferation (ROR-P) outputs from PAM50 were used for analysis. The
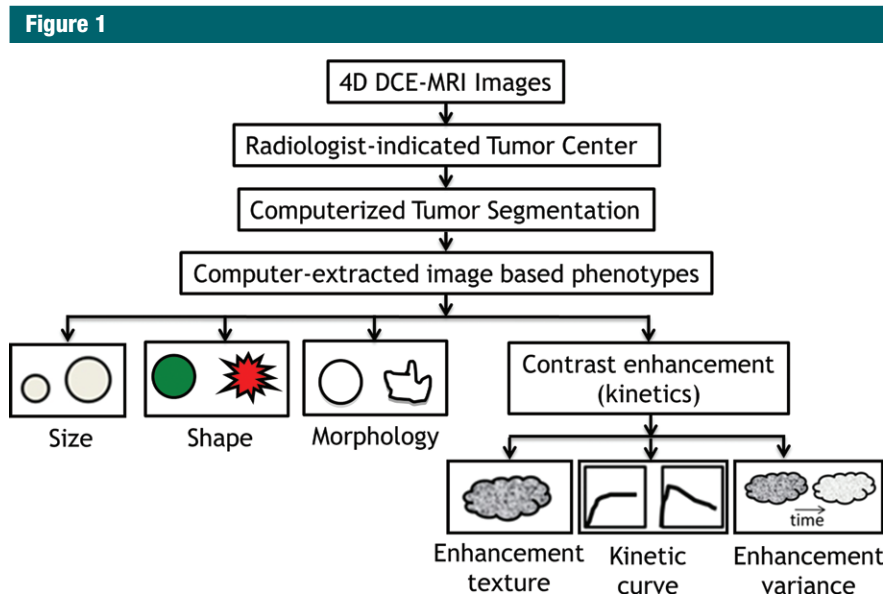
Figure 1: Schematic diagram illustrates the computer extraction of the quantitative MR imaging–based tumor phenotypes. *DCE* = dynamic contrast-enhanced.

research versions of MammaPrint (3) and Oncotype DX (5) were applied to the messenger RNA sequencing data as described previously (28), with the scaling exception used for Oncotype DX noted earlier.

Computerized Quantitative MR Image Analysis of the Tumors

Quantitative MR imaging radiomics analysis was conducted to yield the CEIPs (Fig 1). Note that we do not present here the details of the technical and/or robustness aspects of the computer-extracted MR imaging phenotypes, as they have already been validated and reported through various peer-reviewed publications (29–34).

From the consensus location identified by the radiologists, computerized three-dimensional tumor segmentation was conducted by yielding delineation of each primary breast tumor from the surrounding parenchyma (29). Note that this automated segmentation technique has been used over the past 10 years on hundreds of breast lesions imaged with different MR imaging units, with results comparable to radiologists' delineations (29,34).

By using techniques developed in prior studies, a total of 38 CEIPs of the breast tumors were extracted automatically in three dimensions from the segmented tumors on MR images to describe *(a)* size (linear size, volume, and surface area), *(b)* shape (sphericity and irregularity), *(c)* margin morphologic appearance (margin sharpness, variance of margin sharpness, and variance of radial gradient histogram, which is used to assess tumor spiculation) (30), *(d)* enhancement texture (calculated on the first postcontrast images by using the gray-level co-occurrence matrix, yielding features of homogeneity, entropy, gray-level dependence, and local image variation [33,34]), *(e)* kinetic curve assessment (based on the most enhancing voxels within a lesion and including maximum contrast enhancement, time to peak, uptake rate, washout rate, curve shape index, enhancement at the first contrast-enhanced time point, signal intensity enhancement ratio, total rate variation, and normalized total rate variation [32]), and *(f)* enhancement-variance kinetics (maximum variance of enhancement, time to peak, variance increase rate, and variance decrease rate [31]). Note that these 38 tumor phenotypes

are all automatically extracted from the MR imaging data. More details are located in Table E1 (online).

Association Analysis between MR imaging CEIPs and Multigene Assay Outputs from the Risk of Recurrence Models

By using the MR imaging CEIPs, we conducted multiple linear regression analysis with stepwise feature selection by using the CEIPs as independent variables and the continuous values from the "research-based" MammaPrint, Oncotype DX, PAM50 ROR-S, or PAM50 ROR-P as the response variable (35), with the analysis yielding selected phenotypes. A *P* value of .05 was used as the significance level for the stepwise feature selection. The Holm *t* test was applied to adjust for multiple testing in the regression models (36). For comparison, univariate linear regression analyses were also performed between each individual MR image–based phenotype and the risk of recurrence scores from the recurrence predictor models of MammaPrint, Oncotype DX, PAM50 ROR-S, and PAM50 ROR-P.

Pilot Analysis of the Predictive Ability of the MR Imaging–based Phenotypes for Risk of Recurrence

In clinical practice, distinguishing between good and bad prognosis is of interest; thus, thresholding is conducted on the continuous values of the multigene-assay tests to yield an output of either good or bad prognosis. We assessed four binary classification tasks, each of which is used to predict good versus bad prognosis, by using cutoffs on the multigene test outputs (Table 1)—that is, *(a)* good prognosis versus bad prognosis as determined by using a MammaPrint cutoff, *(b)* low to medium risk of recurrence versus high risk as determined by using an Oncotype DX cutoff, *(c)* low to medium risk of recurrence versus high risk as determined by using a PAM50 ROR-S cutoff, and *(d)* low to medium risk of recurrence versus high risk as determined by using a PAM50 ROR-P cutoff.
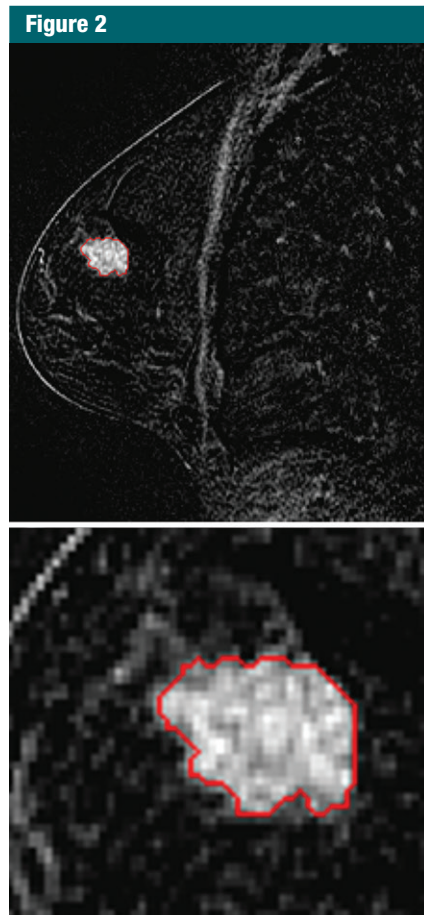
Figure 2

Figure 2: Sagittal MR images in a case with a potentially good prognosis, a 75-year-old woman evaluated as having an ER-positive, PR-positive, HER2-negative, lymph node–negative, stage II invasive breast cancer. The luminal A case is shown, along with the three-dimensional computer segmentation (red overlay) of the primary tumor. The effective diameter, shape irregularity, heterogeneity in terms of entropy, and heterogeneity in terms of maximum correlation coefficient of this tumor are 16.8 mm, 0.438, 6.27, and 0.843, respectively, with ranges of 7.8–54.0 mm, 0.40–0.84, 6.00–6.59, and 0.646–0.925.

For each classification task, a leave-one-case-out cross-validation analysis was conducted with logistic regression to obtain a classifier score for each case (tumor). Within each cross-validation iteration, stepwise feature selection with the Wilks lambda criterion was conducted with subsequent logistic regression classifier fitting on these selected features. To assess the
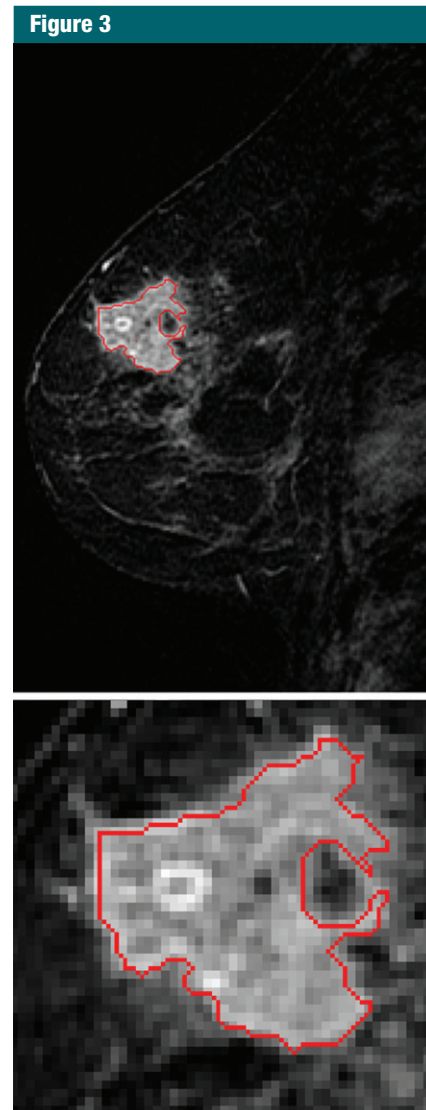
Figure 3

Figure 3: Sagittal MR images in a case with a potentially poor prognosis, a 44-year-old woman evaluated as having an ER-negative, PR-negative, HER2-negative, lymph node–negative, stage II invasive breast cancer. The basal-like case is shown, along with the three-dimensional computer segmentation (red overlay) of the primary tumor. The effective diameter, shape irregularity, heterogeneity in terms of entropy, and heterogeneity in terms of maximum correlation coefficient of this tumor are 21.7 mm, 0.592, 6.51, and 0.732, respectively, with ranges of 7.8–54.0 mm, 0.40–0.84, 6.00–6.59, and 0.646–0.925.

performance of each logistic regression classifier, receiver operating characteristic (ROC) analysis was conducted

Table 2

Associations from Multiple Linear Regression Analysis between CEIPs and Risk of Recurrence Scores

Research Gene Assay	Goodness of Fit	P Value
MammaPrint	$R^2 = 0.30$, $r = 0.55$	<.0001
Oncotype DX	$R^2 = 0.25$, $r = 0.5$	<.0001
PAM50 ROR-S	$R^2 = 0.32$, $r = 0.56$	<.0001
PAM50 ROR-P	$R^2 = 0.28$, $r = 0.53$	<.0001

Note.—R^2 is the coefficient of determination, which indicates how well the data fit a linear model, and r is the correlation coefficient.

Table 3

Associations between CEIPs and Risk of Recurrence Scores according to the Multiple Linear Regression Model

Research Gene Assay and Phenotypic Category	Feature	Regression Coefficient	P Value
MammaPrint	Constant	−9.60	.0070
Enhancement texture	Maximum correlation coefficient	3.14	.00021
Enhancement texture	Sum average	0.22	.011
Size	Effective diameter	−0.020	.0019
Oncotype DX	Constant	161.52	.00073
Kinetic curve assessment	Maximum enhancement	10.30	.014
Enhancement texture	Maximum correlation coefficient	−200.23	.0015
Size	Effective diameter	1.89	.00030
PAM50 ROR-S	Constant	491.36	.012
Enhancement texture	Maximum correlation coefficient	−182.33	.00011
Enhancement texture	Sum average	−9.87	.039
Size	Effective diameter	1.23	.00044
PAM50 ROR-P	Constant	97.51	.0013
Kinetic curve assessment	Uptake rate	384.68	.033
Enhancement texture	Maximum correlation coefficient	−138.98	.00057
Size	Effective diameter	1.35	<.0001

Note.—The Holm t test was applied for correcting of multiple testing.

(by using the semiparametric "proper" binormal ROC model [37–39]) with the classifier scores as the decision variable, with the area under the ROC curve serving as the figure of merit. All analysis routines were written in Mat-Lab (version 8.0, MathWorks, Natick, Mass).

Results

Figures 2 and 3 show examples of MR images in two cases: a case of a potentially good prognosis and a case of a potentially bad prognosis, along with the computer segmentations of the primary tumors. An enlarged view of each tumor is also shown to demonstrate the heterogeneity of uptake values within the tumor. The corresponding CEIP characteristics are also given.

The multiple linear regression analyses demonstrated significant associations ($R^2 = 0.25$–0.32, $r = 0.50$–0.56, $P < .0001$) between selected CEIP signatures and the multigene assay recurrence scores (Tables 2, 3). Key CEIPs from stepwise feature selection included tumor size and enhancement texture, characterizing lesion heterogeneity. Overall, results from all four multiple linear regression analyses indicate that tumors with a high risk of recurrence tend to be larger and show more heterogeneous enhancement patterns.

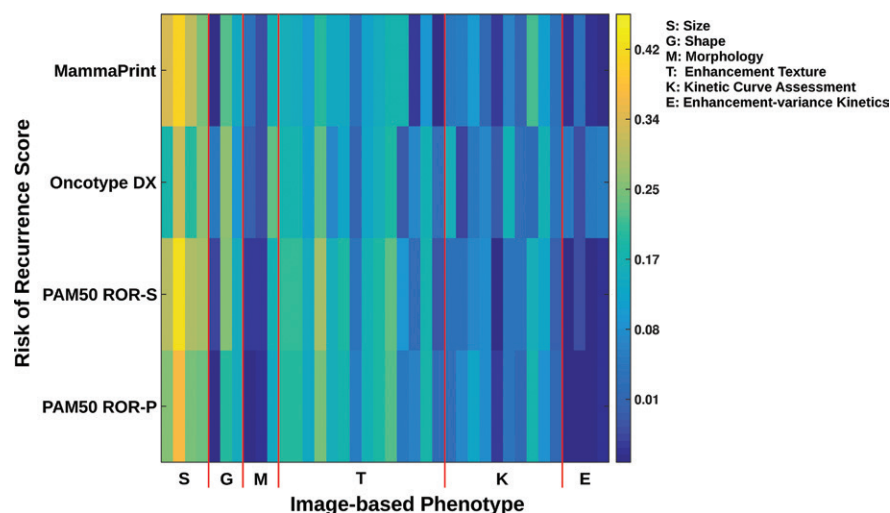A correlation heat map based on univariate linear regression analysis between each individual MR imaging phenotype and the four risks of recurrence scores are shown in Figure 4. Some phenotypes correlate similarly (ie, similar color on the color scale) across the risk estimate models, while others do not.
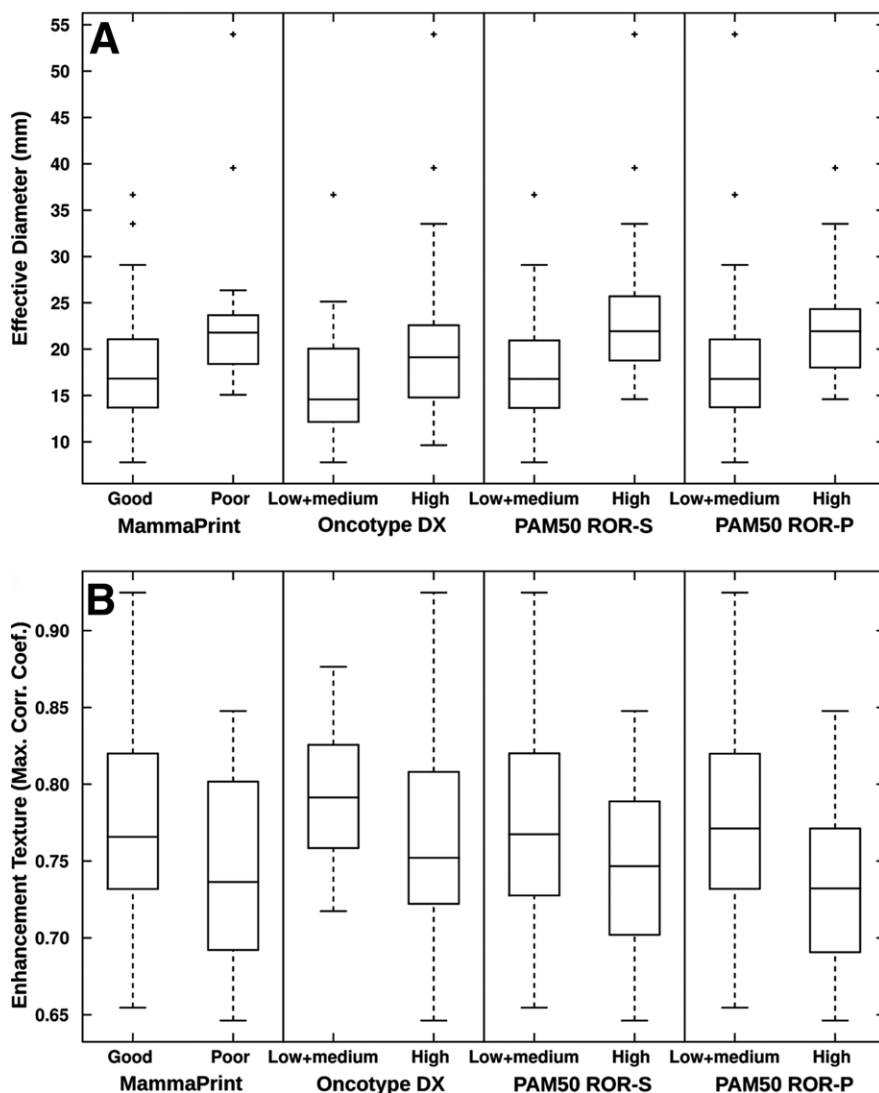
Figure 4

Figure 4: Color map shows the correlation of the MR imaging–based phenotypes with the recurrence predictor models of MammoPrint, Oncotype DX, PAM50 ROR-S, and PAM50 ROR-P. For this color scale, yellow indicates higher correlation as compared with blue. The different gene assays (recurrence predictor models) serve as our "reference standard" in this study.

Positive correlation between the selected MR imaging phenotypes of size (effective diameter) and negative correlation with enhancement texture (maximum correlation coefficient) and increasing levels of risk of

Figure 5

Figure 5: Box and whisker plots show the relationship of the MR imaging–based phenotypes of, *A,* size (effective diameter) and, *B,* enhancement texture (maximum correlation coefficient) with the recurrence predictor models of MammaPrint, Oncotype DX, PAM50 ROR-S, and PAM50 ROR-P. Note that a low value of this texture feature infers a more heterogeneous enhancement pattern.
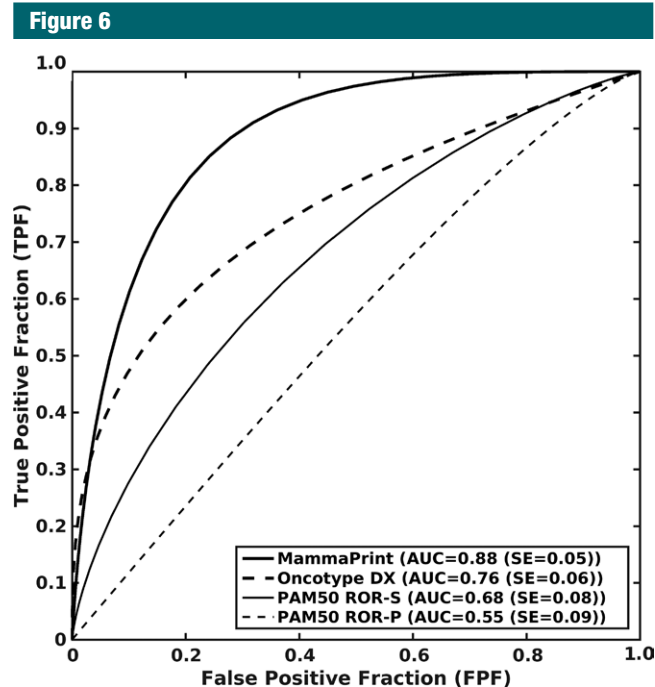
recurrence for MammaPrint, Oncotype DX, PAM50 ROR-S, and PAM50 ROR-P were observed (Fig 5). Note that a low value of this enhancement texture feature infers a more heterogeneous enhancement pattern.

Use of the CEIPs in the tasks of distinguishing between low to medium and high risk levels of recurrence yielded area under the ROC curve values of 0.88 (standard error, 0.05), 0.76 (standard error, 0.06), 0.68 (standard error, 0.08), and 0.55 (standard error, 0.09) for MammaPrint, Oncotype DX, PAM50 ROR-S, and PAM50 ROR-P, respectively, with all but the latter showing statistical difference from chance (Fig 6). Of note, we realize that the Oncotype DX gene assay is usually conducted clinically only in ER-positive cases, but the result shown here is for all cases used in this study.

Discussion

The association analysis between the CEIPs and the risk of recurrence scores from various gene-assay models yielded moderate correlations. The MR imaging phenotypes selected from multiple linear regression analyses were related to breast tumor size, enhancement texture, and characteristics of the kinetic curve. Similar, negatively correlated relationships between the MR imaging phenotype of enhancement texture (maximum correlation coefficient) and the recurrence scores were observed across all four recurrence models. Since enhancement texture is calculated on the MR image acquired at the first postcontrast time point, these enhancement texture phenotypes quantitatively characterize the heterogeneous nature of contrast material uptake within the breast tumor. The smaller the enhancement texture, the more heterogeneous the tumor, which appears to indicate a higher risk of recurrence. Assessment of heterogeneity by using a noninvasive method such as imaging may be important in the future as more targetable agents are used for treating breast cancer and in the neoadjuvant setting in monitoring treatment response. As we understand that breast cancers can be extremely heterogeneous, harboring multiple driver mutations that may change over time, having a method to assess heterogeneity is likely useful. Assessment of heterogeneity may set prognostic expectations and affect treatment options.

Understanding the relationships between gene expression profiles, imaging phenotypes, and outcomes like recurrence risk has the potential to provide insights into the complex cancer biology at work in each individual patient. Currently, gene expression profiles are increasingly helping to distinguish tumor types beyond features that are evident at conventional histopathologic examination. In the future, CEIPs have the potential to compliment these expression profiles by demonstrating anatomic and functional characteristics that might improve prediction of recurrence or other important outcomes. Our finding

Figure 6

Figure 6: ROC curves for the leave-one-case-out logistic regression classifiers by using CEIPs as the decision variable in the tasks of distinguishing between low to medium and high risk levels of recurrence for MammaPrint, Oncotype DX, PAM50 ROR-S, and PAM50 ROR-P, respectively.

that enhancement texture features are consistently associated with recurrence score may indicate that internal tumor architecture, such as microvascular density (ie, tumor-related angiogenesis) and/or central necrosis are playing a biological role that is important in recurrence. While strongly asserting this connection between gene expression and imaging demonstrates that a key to prognosis may be premature on the basis of our current results, understanding these patterns holds promise for untangling how gene expression in concert with in vivo imaging features map to both biological molecular mechanisms and outcomes.

There are some limitations of this study, such as the small data set, since breast MR images are not available for most of the TCGA breast cancer cases. Another limitation was that the scores for risk of recurrence (MammaPrint, Oncotype DX, and PAM50) were obtained from research-based determinations and not from the actual clinical tests, although one would

expect similar results (3–9). Also, we only analyzed dynamic contrast-enhanced MR images and not T2-weighted or diffusion-weighted images. One would expect improved performance by using multiparametric breast MR images; thus, we will analyze those in the future. In addition, the MR images used in this study were acquired from multiple institutions with various acquisition protocols. Given the improved MR imaging technology and standardized imaging acquisition protocols, we would expect in the future to see even more association with risk of recurrence. Case composition, such as the distribution of ER-positive cases (87%) and ER-negative cases (13%), is different from the general clinical population distribution, which is usually approximately a 2:1 ratio. In addition, there were many "good prognosis" cancer cases in the study. The ground truth used in this study was the estimated risk of recurrence instead of actual survival information, as it was not available for the study. Thus, we had to

use the risk status for a given cancer as the surrogate marker. Also, cases used in this study were predetermined according to TCGA inclusion criteria. Most women in this study had core biopsy–proven invasive breast cancer before undergoing MR imaging examinations, which may confound our findings in this study in terms of heterogeneity in enhancement pattern. Thus, the results in this study need further validation in a larger data set to better assess its potential clinical use in the future. Even with these limitations, the TCGA data set is currently still the largest publicly available data set for this radiomics research.

In conclusion, the results in this study indicate that quantitative MR imaging radiomics shows promise as a means for image-based phenotyping in assessing the risk of cancer recurrence. Merging imaging phenotypes with genomic data in the future may lead to improved survival predictors. Such quantitative radiomic prognostic models of breast cancer may potentially be useful for precision medicine and affect patient treatment strategy.

References

1. Osin P, Shipley J, Lu YJ, Crook T, Gusterson BA. Experimental pathology and breast cancer genetics: new technologies. Recent Results Cancer Res 1998;152:35–48.

2. Unger MA, Weber BL. Recent advances in breast cancer biology. Curr Opin Oncol 2000;12(6):521–525.

3. van 't Veer LJ, Dai H, van de Vijver MJ, et al. Gene expression profiling predicts clinical outcome of breast cancer. Nature 2002;415 (6871):530–536.

4. van de Vijver MJ, He YD, van't Veer LJ, et al. A gene-expression signature as a predictor of survival in breast cancer. N Engl J Med 2002;347(25):1999–2009.

5. Paik S, Shak S, Tang G, et al. A multigene assay to predict recurrence of tamoxifen-treated, node-negative breast cancer. N Engl J Med 2004;351(27):2817–2826.

6. Paik S, Tang G, Shak S, et al. Gene expression and benefit of chemotherapy in women with node-negative, estrogen receptor-positive breast cancer. J Clin Oncol 2006;24(23): 3726–3734.

7. Cronin M, Sangli C, Liu M-L, et al. Analytical validation of the Oncotype DX genomic diagnostic test for recurrence prognosis and therapeutic response prediction in node-negative, estrogen receptor-positive breast cancer. Clin Chem 2007;53(6):1084–1091.

8. Parker JS, Mullins M, Cheang MCU, et al. Supervised risk predictor of breast cancer based on intrinsic subtypes. J Clin Oncol 2009;27(8):1160–1167.

9. Prat A, Parker JS, Fan C, Perou CM. PAM50 assay and the three-gene model for identifying the major and clinically relevant molecular subtypes of breast cancer. Breast Cancer Res Treat 2012;135(1):301–306.

10. Giger ML. Update on the potential of computer-aided diagnosis for breast cancer. Future Oncol 2010;6(1):1–4.

11. Giger ML, Chan H-P, Boone J. Anniversary paper: history and status of CAD and quantitative image analysis: the role of medical physics and AAPM. Med Phys 2008;35(12):5799–5820.

12. Giger ML, Karssemeijer N, Schnabel JA. Breast image analysis for risk assessment, detection, diagnosis, and treatment of cancer. Annu Rev Biomed Eng 2013;15: 327–357.

13. Bhooshan N, Giger ML, Jansen SA, Li H, Lan L, Newstead GM. Cancerous breast lesions on dynamic contrast-enhanced MR images: computerized characterization for image-based prognostic markers. Radiology 2010;254(3):680–690.

14. Bhooshan N, Giger M, Edwards D, et al. Computerized three-class classification of MRI-based prognostic markers for breast cancer. Phys Med Biol 2011;56(18):5995–6008.

15. Yang Q, Li L, Zhang J, Shao G, Zheng B. A computerized global MR image feature analysis scheme to assist diagnosis of breast cancer: a preliminary assessment. Eur J Radiol 2014;83(7):1086–1091.

16. Agner SC, Rosen MA, Englander S, et al. Computerized image analysis for identifying triple-negative breast cancers and differentiating them from other molecular subtypes of breast cancer on dynamic contrast-enhanced MR images: a feasibility study. Radiology 2014;272(1):91–99.

17. Youk JH, Son EJ, Chung J, Kim JA, Kim EK. Triple-negative invasive breast cancer on dynamic contrast-enhanced and diffusion-weighted MR imaging: comparison with other breast cancer subtypes. Eur Radiol 2012;22(8):1724–1734.

18. Mazurowski MA, Zhang J, Grimm LJ, Yoon SC, Silber JI. Radiogenomic analysis of breast cancer: luminal B molecular subtype is associated with enhancement dynamics at MR imaging. Radiology 2014;273(2):365–372.

19. Ashraf AB, Daye D, Gavenonis S, et al. Identification of intrinsic imaging phenotypes for breast cancer tumors: preliminary associations with gene expression profiles. Radiology 2014;272(2):374–384.

20. Huo Z, Giger ML, Olopade OI, et al. Computerized analysis of digitized mammograms of BRCA1 and BRCA2 gene mutation carriers. Radiology 2002;225(2):519–526.

21. Li H, Giger ML, Lan L, et al. Computerized analysis of mammographic parenchymal patterns on a large clinical dataset of full-field digital mammograms: robustness study with two high-risk datasets. J Digit Imaging 2012;25(5):591–598.

22. Li H, Giger ML, Sun C, et al. Pilot study demonstrating potential association between breast cancer image-based risk phenotypes and genomic biomarkers. Med Phys 2014;41(3):031917.

23. Gierach GL, Li H, Loud JT, et al. Relationships between computer-extracted mammographic texture pattern features and BRCA1/2 mutation status: a cross-sectional study. Breast Cancer Res 2014;16(4):424.

24. Cancer Genome Atlas Network. Comprehensive molecular portraits of human breast tumours. Nature 2012;490(7418):61–70.

25. Clark K, Vendt B, Smith K, et al. The Cancer Imaging Archive (TCIA): maintaining and operating a public information repository. J Digit Imaging 2013;26(6):1045–1057.

26. Mongkolwat P, Kleper V, Talbot S, Rubin D. The National Cancer Informatics Program (NCIP) Annotation and Image Markup (AIM) Foundation model. J Digit Imaging 2014;27(6):692–701.

27. Fan C, Oh DS, Wessels L, et al. Concordance among gene-expression-based predictors for breast cancer. N Engl J Med 2006;355(6):560–569.

28. Fan C, Prat A, Parker JS, et al. Building prognostic models for breast cancer patients using clinical variables and hundreds of gene expression signatures. BMC Med Genomics 2011;4:3.

29. Chen W, Giger ML, Bick U. A fuzzy c-means (FCM)-based approach for computerized segmentation of breast lesions in dynamic contrast-enhanced MR images. Acad Radiol 2006;13(1):63–72.

30. Gilhuijs KGA, Giger ML, Bick U. Computerized analysis of breast lesions in three dimensions using dynamic magnetic-resonance imaging. Med Phys 1998;25(9):1647–1654.

31. Chen W, Giger ML, Lan L, Bick U. Computerized interpretation of breast MRI: investigation of enhancement-variance dynamics. Med Phys 2004;31(5):1076–1082.

32. Chen W, Giger ML, Bick U, Newstead GM. Automatic identification and classification of characteristic kinetic curves of breast lesions

on DCE-MRI. Med Phys 2006;33(8):2878–2887.

33. Chen W, Giger ML, Li H, Bick U, Newstead GM. Volumetric texture analysis of breast lesions on contrast-enhanced magnetic resonance images. Magn Reson Med 2007; 58(3):562–571.

34. Chen W, Giger ML, Newstead GM, et al. Computerized assessment of breast lesion malignancy using DCE-MRI robustness study on two independent clinical datasets from two manufacturers. Acad Radiol 2010;17(7):822–829.

35. Draper NR, Smith H. Applied regression analysis. Hoboken, NJ: Wiley-Interscience, 1998; 307–312.

36. Holm S. A simple sequentially rejective multiple test procedure. Scand J Stat 1979;6(2): 65–70.

37. Metz CE, Pan X. "Proper" binormal ROC curves: theory and maximum-likelihood estimation. J Math Psychol 1999;43(1):1–33.

38. Pan X, Metz CE. The "proper" binormal model: parametric receiver operating characteristic curve estimation with de-generate data. Acad Radiol 1997;4(5):380–389.

39. Pesce LL, Metz CE. Reliable and computationally efficient maximum-likelihood estimation of "proper" binormal ROC curves. Acad Radiol 2007;14(7):814–829.